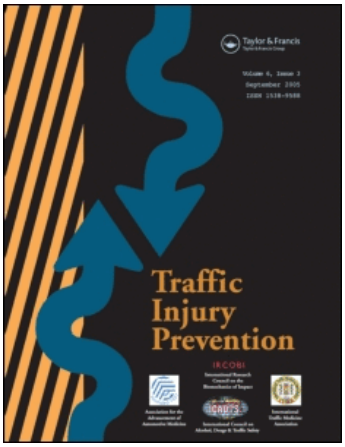

Traffic Injury Prevention
Publication details, including instructions for authors and subscription information:
http://www.informaworld.com/smpp/title~content=t713456148

Cervical Spine Loads and Intervertebral Motions During Whiplash

Paul C. Ivancic[a]; Manohar M. Panjabi[a]; Shigeki Ito[b]
[a] Department of Orthopaedics and Rehabilitation, Biomechanics Research Laboratory, Yale University School of Medicine, New Haven, Connecticut, USA [b] Department of Orthopaedic Surgery, St. Marianna University School of Medicine, Kanagawa, Japan

To cite this Article Ivancic, Paul C. , Panjabi, Manohar M. and Ito, Shigeki(2006) 'Cervical Spine Loads and Intervertebral Motions During Whiplash', Traffic Injury Prevention, 7: 4, 389 — 399
To link to this Article: DOI: 10.1080/15389580600789127
URL: http://dx.doi.org/10.1080/15389580600789127

Traffic Injury Prevention, 7:389–399, 2006

ISSN: 1538-9588 print / 1538-957X online
DOI: 10.1080/15389580600789127

Taylor & Francis
Taylor & Francis Group

Cervical Spine Loads and Intervertebral Motions During Whiplash

PAUL C. IVANCIC and MANOHAR M. PANJABI

Biomechanics Research Laboratory, Department of Orthopaedics and Rehabilitation, Yale University School of Medicine, New Haven, Connecticut, USA

SHIGEKI ITO

Department of Orthopaedic Surgery, St. Marianna University School of Medicine, Kanagawa, Japan

Objective. *To quantify the dynamic loads and intervertebral motions throughout the cervical spine during simulated rear impacts.*

Methods. *Using a biofidelic whole cervical spine model with muscle force replication and surrogate head and bench-top mini-sled, impacts were simulated at 3.5, 5, 6.5, and 8 g horizontal accelerations of the T1 vertebra. Inverse dynamics was used to calculate the dynamic cervical spine loads at the centers of mass of the head and vertebrae (C1-T1). The average peak loads and intervertebral motions were statistically compared ($P < 0.05$) throughout the cervical spine.*

Results. *Load and motion peaks generally increased with increasing impact acceleration. The average extension moment peaks at the lower cervical spine, reaching 40.7 Nm at C7-T1, significantly exceeded the moment peaks at the upper and middle cervical spine. The highest average axial tension peak of 276.9 N was observed at the head, significantly greater than at C4 through T1. The average axial compression peaks, reaching 223.2 N at C5, were significantly greater at C4 through T1, as compared to head-C1. The highest average posterior shear force peak of 269.5 N was observed at T1.*

Conclusion. *During whiplash, the cervical spine is subjected to not only bending moments, but also axial and shear forces. These combined loads caused both intervertebral rotations and translations.*

Keywords Whiplash Biomechanics; Dynamics; Loads; Rear Impact; Cervical Spine

Neck injury due to whiplash continues to result in significant societal costs, estimated as high as $29 billion annually (Freeman et al., 1999). Epidemiological observations have found that the risk of sustaining soft-tissue neck injury was greatest in rear-impact collisions, as compared with other impact configurations (Jakobsson et al., 2000; Spitzer et al., 1995). Recent studies of dynamic neck kinematics and ligamentous strains during simulated rear impacts have lead to improved understanding of spinal kinematics and potential soft-tissue injury sites (Cusick et al., 2001; Panjabi et al., 2004a; Pearson et al., 2004). However, comprehensive understanding of whiplash injury mechanisms is possible only with combined knowledge of dynamic loads and motions at each cervical spinal level during trauma.

Although the dynamic spinal motions throughout the cervical spine have been extensively reported, there remains a lack of similar data concerning the spinal loads. In vivo dynamic loads at the occipital condyles have been computed using inverse dynamics and head motion, acceleration, mass, and inertia data (Davidsson et al., 1999; Mertz & Patrick, 1967, 1971; Ono et al., 1997; Siegmund et al., 2001; van den Kroonenberg et al., 1998). Even during in vitro simulations, only the loads at the occipital condyles in whole cadavers (Luan et al., 2000; Yoganandan et al., 2000) and at a load cell mounted at the base of a head-T1 specimen were reported (Stemper et al., 2003; Yoganandan & Pintar, 1997). Lastly, loads calculated using mathematical models have been reported only at the occipital condyles or T1 vertebra (Garcia & Ravani, 2003; Tencer et al., 2002; van der Horst, 2002).

In summary, no previous biomechanical study has reported both the neck loads and motions at each spinal level during rear impacts. Such data is necessary to understand whiplash injury mechanisms, develop vertebral load-based injury criteria, and provide a baseline from which to compare the effects of neck injury prevention systems during whiplash trauma. The goals of this study were to: 1) calculate the dynamic vertebral loads throughout the cervical spine using inverse dynamics and 2) calculate the dynamic intervertebral motions during simulated rear impacts of a biofidelic whole cervical spine model with muscle force replication and surrogate head (Ivancic et al., 2005b). We hypothesized that significant differences existed in peak

Received 18 November 2005; accepted 4 April 2006.

Address correspondence to Paul C. Ivancic, Biomechanics Research Laboratory, Department of Orthopaedics and Rehabilitation, Yale University School of Medicine, 333 Cedar St., P.O. Box 208071, New Haven CT 06520-8071, USA. E-mail: paul.ivancic@yale.edu

dynamic vertebral loads and intervertebral motions throughout the cervical spine.

METHODS

Overview

The anatomic coordinate systems used to express the dynamic cervical spine loads and motions are first described, followed by specimen preparation for rear-impact simulation. The complete description of the model (Ivancic et al., 2005b) and peak dynamic intervertebral rotation data (Panjabi et al., 2005a) have been published in separate manuscripts. In the present study, inverse dynamics was used to calculate the dynamic loads at the CoM of the head and each vertebra during whiplash, using the measured dynamic head and vertebral kinematics, accelerations, and load cell data, and mass and inertia properties obtained from literature. Error analyses were performed.

Anatomic Coordinate Systems, Loads, and Motions

For the head/C1 to C7/T1 spinal levels, anatomic coordinate systems, xyz_i, where i is the head or a vertebra, were defined (Figure 1). The positive z-axis was oriented anteriorly while the positive y-axis was oriented superiorly, and the positive x-axis to the left. The vertebral loads included moments of sagittal flexion (+Mx) and extension (−Mx), and forces of axial tension (+Fy), axial compression (−Fy), anterior shear (+Fz), and posterior shear (−Fz) at the center of mass (CoM) of the head and each vertebra. The intervertebral motions included rotations of sagittal flexion (+Rx) and extension (−Rx), and translations of axial separation (+Ty), axial compression (−Ty), anterior shear (+Tz), and posterior shear (−Tz) at the CoM of the head and each vertebra. The forces and translations at the CoM of the superior mass were expressed in the coordinate system of the directly inferior mass. The head coordinate system had its origin fixed to the posterior edge of the foramen magnum with its z-axis oriented anteriorly though anterior edge of foramen magnum, while its positive y-axis was oriented superiorly (Figure 2). The C1 coordinate system had its origin at the posterior border of the posterior arch, while the coordinate systems at C2 to T1 had their origins at the posteroinferior corners of the vertebral bodies.

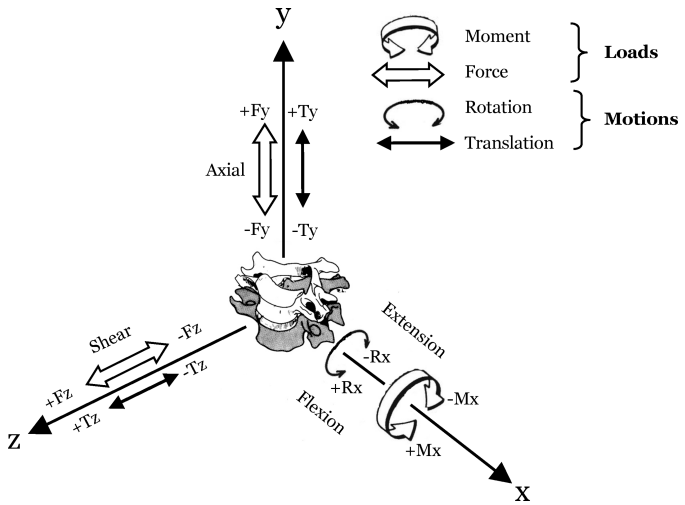

Figure 1 The nomenclature for loads and motions. The vertebral loads include moments of sagittal flexion (+Mx) and extension (−Mx), and forces of axial tension (+Fy), axial compression (−Fy), anterior shear (+Fz), and posterior shear (−Fz) at the center of mass (CoM) of the head and vertebrae. The intervertebral motions include rotations of sagittal flexion (+Rx) and extension (−Rx), and translations of axial separation (+Ty), axial compression (−Ty), anterior shear (+Tz), and posterior shear (−Tz) of the CoM of the head and vertebrae. The forces and translations at the CoM of the superior mass were expressed in the coordinate system of the directly inferior mass. Modified from White and Panjabi (1990).

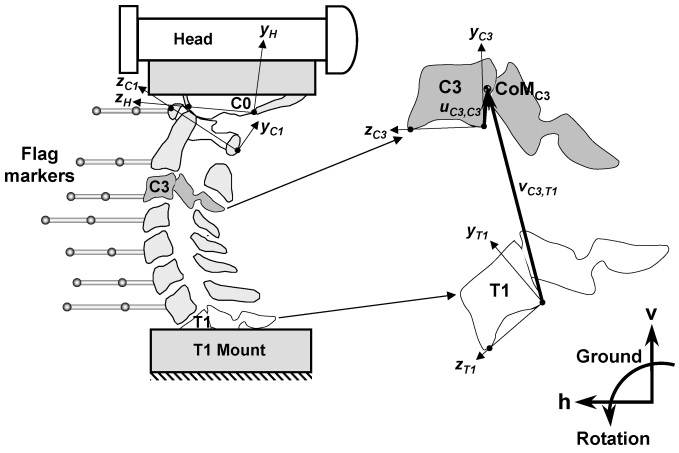

Figure 2 A schematic of the whole cervical spine and anatomic coordinate systems, z_i, y_i, established from the radiographs. For the sake of clarity, the muscle force replication is not shown. The head (H) and vertebral (C1 to T1) CoM coordinates were expressed in both the local i coordinate system fixed to each vertebra and the spinal T1 coordinate system in Table IA. As an example, the vectors $\boldsymbol{u}_{C3,C3}$ and $\boldsymbol{v}_{C3,T1}$ define the C3 CoM in the C3 local- and spinal-coordinate system, respectively. The ground coordinate system, hv, had its h-axis oriented horizontally and v-axis oriented vertically, with counter-clockwise rotation being positive. Modified from Ivancic et al. (2005b).

Specimen Preparation

Six fresh-frozen human osteoligamentous whole cervical spine specimens (occiput-T1) were mounted in resin at the occiput and T1 in normal neutral posture as defined in Table IA. The average age of the specimens was 70.8 years (range, 52 to 84 years) and there were four male and two female donors. Apart from typical age related changes, the specimens did not suffer from any disease that could have affected the osteoligamentous structures. Lightweight motion-tracking flags were rigidly attached to each vertebra (C1 to C7) and to the occipital and T1 mounts (Figure 2). A surrogate head, attached to the occipital mount, and the spine were stabilized using compressive muscle force replication (MFR). The model, described in detail elsewhere, has been validated against in vivo simulated whiplash data (Ivancic et al., 2005b).

Rear-Impact Simulation and Monitoring

Rear-impact simulation was performed using a previously developed bench-top sled apparatus (Panjabi et al., 1998). The incremental trauma protocol was used at nominal peak T1 horizontal

Table I Head and vertebral CoMs, mass properties, and inclinations of coordinate systems in neutral posture. A) Average (SD) head (H) and vertebral (C1 to T1) center of mass (CoM) coordinates (mm) expressed in local i coordinate system fixed to each vertebra and in T1 coordinate system (see Figure 2) (van der Horst, 2002) and inclinations (degrees) of z-axis relative to h-axis of ground coordinate system. $z_{i,i}$ and $y_{i,i}$ represent CoM coordinates of mass i in local i coordinate system, while $z_{i,T1}$ and $y_{i,T1}$ represent CoM coordinates of mass i in T1 coordinate system. A positive inclination indicates anterior tilt, while negative indicates posterior tilt. B) Head and vertebral masses (kg) and sagittal mass moments of inertia (kg m^2) used in inverse dynamics model. The surrogate head properties were measured, while the vertebral properties were obtained from the literature (Camacho et al., 1997)

A. CoMs and Inclinations of Coordinate Systems in Neutral Posture

	CoM (mm) local		CoM (mm) relative to T1		Inclination
i	$z_{i,i}$	$y_{i,i}$	$z_{i,T1}$	$y_{i,T1}$	(degrees)
H	46.0 (9.0)	64.8 (5.3)	−76.9 (23.5)	195.9 (18.3)	−27.2 (8.8)
C1	31.2 (4.2)	1.9 (1.4)	−29.8 (16.6)	128.3 (16.6)	−28.6 (9.8)
C2	−1.0 (1.2)	5.9 (1.0)	−18.8 (14.5)	109.7 (12.8)	0.7 (11.1)
C3	−0.8 (0.8)	7.1 (0.7)	−12.0 (12.8)	94.4 (12.2)	6.0 (8.9)
C4	−0.3 (1.4)	6.7 (1.0)	−6.0 (9.6)	78.0 (9.9)	13.2 (7.4)
C5	0.1 (1.1)	6.3 (1.5)	−2.3 (5.7)	61.8 (7.6)	14.7 (6.0)
C6	0.2 (1.7)	6.4 (0.9)	1.6 (2.6)	46.1 (5.1)	15.9 (5.4)
C7	−0.2 (2.1)	7.1 (1.1)	2.3 (1.2)	28.4 (3.0)	20.2 (7.9)
T1	1.6 (1.4)	8.5 (1.2)	1.6 (1.4)	8.5 (1.2)	17.6 (9.0)

B. Mass Properties

	Mass (kg)	Mass moment of inertia (kg m^2)
H	3.30E+00	1.60E−02
C1	4.04E−02	6.33E−06
C2	5.08E−02	1.10E−05
C3	3.63E−02	4.50E−06
C4	3.66E−02	4.71E−06
C5	3.71E−02	4.92E−06
C6	4.39E−02	6.86E−06
C7	5.05E−02	1.19E−05
T1	5.05E−02	Not applicable

accelerations of 3.5, 5, 6.5, and 8 g (Ghole et al., 2004). No head restraint was used to limit head extension, however a soft stop was provided to protect the spine from injury during flexion rebound. A bi-axial accelerometer (part no. ADXL250JQC, Analog Devices, Norwood, MA, USA) was mounted to the sled to determine the T1 horizontal acceleration. The horizontal axis of the T1 accelerometer was oriented along the h-axis of the ground coordinate system. A six-component load cell (MC3A Force/Torque Sensor; load capacities of Fh: 2200 N, Fv: 4400 N, and sagittal moment: 110 Nm; Advanced Mechanical Technology, Inc., Watertown, MA) was rigidly connected between the T1 mount and the sled. The T1 horizontal acceleration and dynamic loads were continuously sampled at 1 kHz using an analog-to-digital converter and a personal computer. The spinal motions were recorded immediately following impact at 500 frames/sec using high-speed digital cameras (Fastcam, Super 10 K, model PS-110, Eastman Kodak Co, Rochester, NY).

Inverse Dynamics

Head and Vertebral Geometry and Kinematics. Custom Matlab programs (Matlab, The Mathworks Inc., Natick, MA, USA) were written to obtain the sagittal coordinates of the flag markers with sub-pixel accuracy in the ground coordinate system for all high-speed movie frames during whiplash (Panjabi et al., 2005a). The dynamic rotations of the head and of each vertebra (C1 to C7) were computed as functions of time during whiplash in the ground coordinate system, hv (Figure 2). A lateral radiograph of each intact specimen in the neutral posture, together with radio-opaque scale markers positioned in the mid-sagittal plane and vertebral motion tracking flags, was taken and digitally scanned to develop geometric relationships between the flag marker centers and the head and vertebral CoMs (Table IA). The latter data were obtained from literature (van der Horst, 2002). The geometric relationships were superimposed onto the neutral posture frame of the high-speed movie. For each subsequent frame, the translations of the head and vertebral CoMs were calculated in the ground coordinate system using the flag translations, rotations, and geometric relationships (Ivancic et al., 2006b).

Head and Vertebral Accelerations. The linear (horizontal and vertical) and angular accelerations of the head and vertebral CoMs were computed in the ground coordinate system by numerical double differentiation of the corresponding motion data, while the T1 horizontal acceleration was measured by the accelerometer.

Head and Vertebral Masses and Mass Moments of Inertias. The specimens of the present study, with an average age of 70.8 years, were weaker than the population most likely to suffer whiplash trauma. To ensure that no specimen was prematurely injured due to excessive head inertia loads, a 3.3 kg surrogate head mass was used (Table IB), which was at the lower end of values measured from cadavers, ranging between 2.8 and 5.8 kg (Becker, 1972; Walker et al., 1973). The vertebral mass and mass moment of inertia data were obtained from a previous study that used the National Library of Medicine's Visible Human Data Set (Camacho et al., 1997).

Load-Cell Data. The six-component load cell was positioned between the T1 mount and the sled. Of the six load components, only the sagittal moment and horizontal and vertical forces were utilized.

Head and Vertebral Loads. Inverse dynamics was used to calculate the dynamic head and vertebral loads during whiplash using the Newton-Euler equations and the aforementioned data. The equations were: $\sum \boldsymbol{F} = m\boldsymbol{a}$ and $\sum M = I\alpha$, where $\boldsymbol{F}$ is the force vector, m is the mass, $\boldsymbol{a}$ is the linear acceleration vector, M is the sagittal bending moment, I is the mass moment of inertia, and α is the sagittal angular acceleration. To calculate the loads at the T1 CoM, a free body diagram from the load cell sensor to the T1 vertebral CoM was constructed, taking into account the mass magnitudes and CoM coordinates of the part of the load cell above the sensor, T1 mount, and part of T1 vertebra below the T1 CoM. Next, the loads at the CoMs at C7 to head were calculated sequentially using similar methodology, taking into account the head and vertebral masses and mass moments of inertia. The dynamic loads were also calculated caudally, beginning from the calculated loads at the head CoM. The maximum average

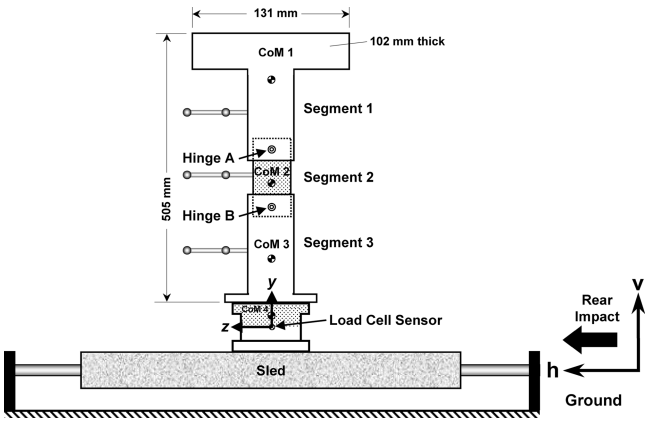

Figure 3 A schematic of the custom jig used to evaluate the errors of the calculated loads and linear accelerations. The jig consisted of three segments of known CoMs (Table IIA), masses and mass moments of inertia (Table IIB), connected by hinge joints. A six-component load cell was rigidly fixed between segment 3 and the sled. Inverse dynamics was used to calculate the dynamic loads at CoM 1, 2, 3, and load-cell sensor during the 4.8 g rear impact. As the load-cell sensor was within the load cell, a fourth segment was defined consisting of that part of the load cell above the load-cell sensor. Its properties are also given in Table II.

difference in the peak loads at the load-cell sensor between the two approaches was 1.3%. All reported dynamic load data were calculated using the former approach.

Error Analyses. A custom jig (Figure 3), consisting of three segments of known masses, sagittal mass moments of inertia and CoM coordinates (Table II), was constructed to evaluate the errors in the computations of vertebral loads and linear accelerations. As the load-cell sensor was within the load cell, a fourth segment was defined consisting of the part of the load cell above the load-cell sensor. The segments were connected by hinge joints, and a motion-tracking flag was rigidly attached to each segment. The base of the jig was rigidly fixed to the load cell on the whiplash sled, which was rear impacted at a peak sled acceleration of 4.8 g. The load-cell data and high-speed camera images were recorded. Using the methodology described above, the dynamic loads at the segment CoMs were calculated using two approaches. First, beginning from the measured load at the load cell, loads were calculated at CoM 3, followed by CoM 2 and CoM 1. Second, beginning from calculated inertial load at CoM 1, the loads at CoM 2, followed by CoM 3, and load-cell sensor, were calculated. The error in the calculated loads was defined as the average difference between the loads calculated at CoM 1, CoM 2, CoM 3, and load-cell sensor using the two approaches. The error in the calculated linear acceleration was defined as the average difference between the sled horizontal acceleration measured by the accelerometer and calculated by numerical double differentiation of the horizontal translation of a flag marker fixed to segment 3. The error data were averaged over the 500 ms time period (250 readings) following the onset of the sled acceleration.

The average errors were small. The average (SD) errors in the calculated horizontal and vertical forces were 0.5 N (1.8 N) and −0.1 N (2.2 N), respectively, while that for the calculated moment ranged between −0.5 Nm (0.5 Nm) at the load-cell sensor and 0.7 Nm (0.7 Nm) at CoM 1. The average error in the linear acceleration was −0.04 g (0.07 g). The average errors in the calculations of the intervertebral rotations and translations, as determined in separate studies, were 0.05° (SD 0.27°) (Panjabi et al., 2004b) and 0.3 mm (SD 0.2 mm) (Pearson et al., 2004), respectively.

Table II The jig (Figure 3). A) Coordinates (mm) of the jig segment CoMs and the hinges in the initial posture in the load-cell coordinate system, zy, and B) segment masses (kg) and sagittal mass moments of inertia (kg m^2). The jig was used to determine the errors in the calculated loads and linear accelerations

A. Coordinates of CoMs and Hinges in Initial Posture

	Coordinates (mm) in load cell coordinate system	
	z	*y*
Hinge A	0.0	294.1
Hinge B	0.0	183.6
CoM 1	0.0	467.6
CoM 2	0.0	227.7
CoM 3	0.0	85.5
CoM 4	0.0	23.2

B. Mass Properties

	Mass (kg)	Mass moment of inertia (kg m^2)
Segment 1	1.21E+00	4.93E−03
Segment 2	1.86E−01	1.85E−04
Segment 3	7.95E−01	Not applicable
Segment 4	3.07E−01	Not applicable

Data Analyses

Filter Specifications. A third order, dual pass, Butterworth low-pass filter with a cutoff frequency of 30 Hz was used to filter all load and motion data. Residual and Fourier analyses demonstrated that most of the signal power was contained under 20 Hz.

Load and Motion Peaks. The dynamic moments and forces at the head and vertebrae (C1 to T1) and the intervertebral rotations (Panjabi et al., 2005a) and translations at head/C1 to C7/T1 were computed as functions of time. For head/C1 to C7/T1 (Figure 1), the forces and translations at the CoM of the superior mass were expressed in the coordinate system of the directly inferior mass. The load and motion peaks were determined during the head extension period (from the onset of the T1 horizontal acceleration to the return of the head to neutral posture). The times of occurrence of all peaks during the 5 g impact, relative to the onset of the T1 horizontal acceleration, were also determined.

Statistics. Single factor (spinal level), repeated measures ANOVA ($P < 0.05$) and Bonferonni pair-wise post-hoc tests (Minitab Rel. 13, Minitab, State College, PA, USA) were used to determine differences in the average peak loads and motions between spinal levels for each impact. Adjusted P-values were computed based upon the number of post hoc tests performed.

RESULTS

A Representative Example

In this example of rear impact (Figure 4), the measured peak T1 horizontal acceleration was 4.7 g and the acceleration pulse duration was 104 ms. Following impact, the loads at head/C1 in the initial 125 ms (Figure 4A) included +Mx, +Fy and −Fz peaks. These loads caused peak +Rx, +Ty and −Tz. Subsequently, −Mx, −Fy, −Rx, and −Ty peaks were observed. At C3/4 (Figure 4B), an initial +Fy peak was observed, followed by −Fz, −Mx, and −Fy peaks. These loads produced −Tz and −Rx. At C6/7 (Figure 4C) all load peaks were observed prior to all motion peaks. The +Fy peak was observed first, followed by the −Fz, −Mx, and −Fy peaks. These loads produced motions of −Rx and −Tz.

The Six Specimens

The average (SD) measured T1 horizontal acceleration peaks during the impacts were 3.6 (0.1), 4.7 (0.3), 6.6 (0.2), and 7.9 (0.3) g, corresponding to the nominal peaks of 3.5, 5, 6.5, and 8 g, respectively. The respective average measured T1 velocity peaks were 9.1 (0.1), 11.4 (0.2), 12.4 (0.3), and 13.1 (0.3) kph. The average duration of the T1 horizontal acceleration pulse was 103.8 (11.0) ms.

Head and Vertebral Loads. The average peak loads at the CoMs of the head and vertebrae (C1 to T1) are presented in tabular form, together with significant differences between the head and vertebral levels for each impact (Tables IIIA to IVC). The peak loads generally increased with increasing impact acceleration. +Mx peaks were not observed inferior to C3 (Table IIIA). The +Mx peaks decreased, while the −Mx peaks increased caudally (Table IIIB). The highest −Mx peak of 40.7 Nm was observed at both C7 and T1 during the 8 g impact. The −Mx peaks at the head were significantly less than at all vertebral levels, which was true for all impacts. The +Fy peaks generally decreased caudally, while the −Fy peaks increased (Tables IVA and IVB). The +Fy peaks at head to C4 were significantly greater than at C6 to T1 for all impacts, except 3.5 g. The highest +Fy peak of 276.9 N was observed at the head during the 8 g impact. The −Fy peaks at C4 to T1 were significantly greater than at head and C1 during all impacts. The highest −Fy peak of 223.2 N was observed at C5 during the 8 g impact. The −Fz peaks generally increased caudally, inferior to the C3 vertebra (Table IVC). The Highest −Fz peak of 269.5 N was observed at T1 during the 8 g impact.

Head/C1 to C7/T1 Motions. The average peak motions are presented in tabular form, together with significant differences between spinal levels for each impact (Tables VA to VIC). The

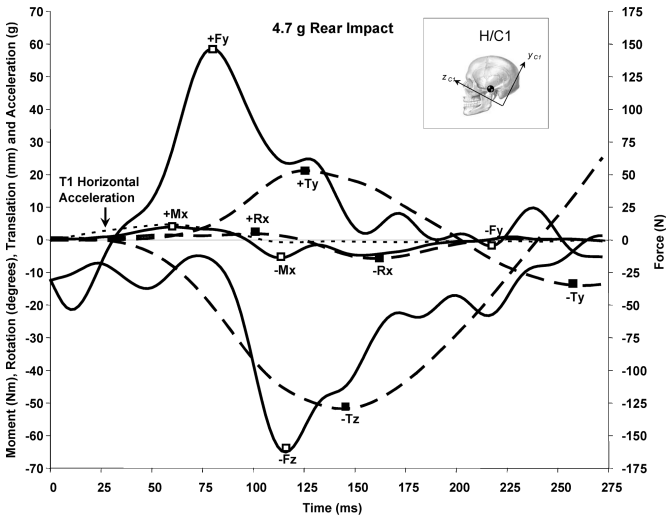

(a)

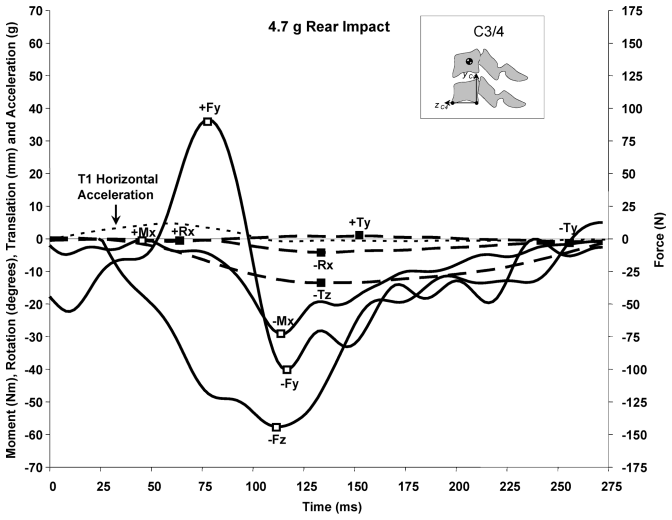

(b)

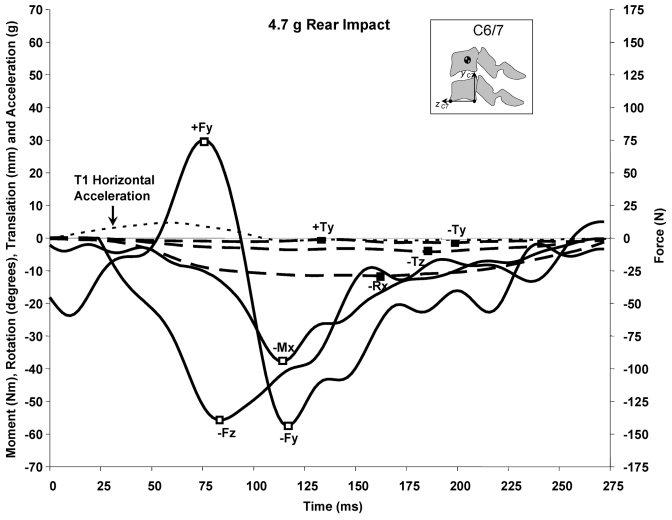

(c)

Figure 4 A representative example of simulated rear impact (specimen #3; 4.7 g) showing the loads and motions vs. time for a) head/C1, b) C3/4, and c) C6/7. The peaks are indicated with open squares (□) for the loads and closed squares (■) for the motions. The T1 horizontal acceleration is also shown. The loads at the CoM of the head are plotted with the head/C1 motions, while the loads at the CoM of the respective upper vertebra are plotted with the intervertebral motions for C3/4 and C6/7. For the nomenclature, see Figure 1.

Table III Moment peaks (Nm). Average (SD) peak A) flexion and B) extension moments at head (H) and vertebral (C1 to T1) centers of mass during rear impacts of 3.5, 5, 6.5, and 8 g. Only significantly different values from the pair-wise comparisons between head and vertebral levels are indicated in the column *Significant*. Blank entries indicate that no significant pair-wise comparisons were observed

	3.5 g		5 g		6.5 g		8 g	
	Moment	Significant	Moment	Significant	Moment	Significant	Moment	Significant
A) Flexion Moment Peaks (+Mx)								
H	3.0 (0.5)	C3	3.7 (0.5)		5.1 (1.3)		7.4 (1.7)	C2-C3
C1	2.5 (1.2)	C3	1.7 (1.7)		4.9 (2.2)		6.4 (2.3)	
C2	1.5 (1.5)		1.6 (0.0)		3.4 (2.4)		4.9 (1.5)	H
C3	0.0 (0.0)	H-C1	1.0 (0.0)		2.2 (2.7)		4.0 (1.3)	H
B) Extension Moment Peaks (−Mx)								
H	4.6 (1.6)	C1-T1	5.6 (1.6)	C1-T1	8.3 (2.1)	C1-T1	13.2 (7.0)	C1-T1
C1	13.6 (3.7)	H,C3-T1	18.7 (4.6)	H,C4-T1	21.7 (6.2)	H,C4-T1	29.2 (14.1)	H,C4-T1
C2	16.0 (4.0)	H,C5-T1	21.0 (5.7)	H,C5-T1	24.2 (6.6)	H,C5-T1	32.5 (14.7)	H,C7-T1
C3	17.8 (4.4)	H-C1,C5-T1	23.3 (6.1)	H,C6-T1	26.4 (7.5)	H, C6-T1	35.0 (16.0)	H
C4	19.6 (4.8)	H-C1,C7-T1	25.6 (6.3)	H-C1,C7-T1	29.1 (7.7)	H-C1,C7-T1	37.4 (16.8)	H-C1
C5	21.5 (5.3)	H-C3	27.9 (6.6)	H-C2	31.9 (8.2)	H-C2	39.0 (17.3)	H-C1
C6	22.9 (5.7)	H-C3	29.5 (6.9)	H-C3	33.8 (8.4)	H-C3	40.5 (16.9)	H-C1
C7	24.1 (6.3)	H-C4	30.8 (7.6)	H-C4	35.5 (8.7)	H-C4	40.7 (16.2)	H-C2
T1	24.8 (7.1)	H-C4	31.8 (7.7)	H-C4	36.9 (8.8)	H-C4	40.7 (12.7)	H-C2

Table IV Force peaks (N). Average (SD) peak A) axial tension, B) axial compression, and C) posterior shear forces at head (H) and vertebral (C1 to T1) centers of mass during rear impacts of 3.5, 5, 6.5, and 8 g. Only significantly different values from the pair-wise comparisons between head and vertebral levels are indicated in the column *Significant*. Blank entries indicate that no significant pair-wise comparisons were observed

	3.5 g		5 g		6.5 g		8 g	
	Force	Significant	Force	Significant	Force	Significant	Force	Significant
A) Axial Tension Peaks (+Fy)								
H	84.1 (19.9)	C1-T1	139.7 (20.8)	C1-T1	207.6 (22.9)	C3-T1	276.9 (25.9)	C4-T1
C1	53.2 (23.0)	H,C5	109.8 (19.5)	H,C4-T1	184.3 (23.2)	C4-T1	259.0 (20.1)	C5-T1
C2	44.6 (24.3)	H	101.5 (13.3)	H,C5-T1	176.9 (22.8)	C5-T1	251.7 (19.2)	C5-T1
C3	34.2 (21.4)	H	87.6 (11.2)	H,C6-T1	162.2 (23.0)	H,C6-T1	237.6 (24.8)	C5-T1
C4	33.0 (15.5)	H	77.3 (15.5)	H-C1,C6-T1	146.4 (25.5)	H-C1,C6-T1	220.1 (31.3)	H,C6-T1
C5	29.1 (12.5)	H,C1	65.6 (20.5)	H-C2,C7-T1	131.3 (32.3)	H-C2,C6-T1	192.3 (46.3)	H-C3,C6-T1
C6	29.3 (17.1)	H	43.4 (21.3)	H-C4	97.8 (33.0)	H-C5	144.1 (49.2)	H-C5
C7	26.9 (12.0)	H	36.7 (22.6)	H-C5	79.5 (35.7)	H-C5	116.2 (49.3)	H-C5
T1	26.3 (12.1)	H	35.9 (22.5)	H-C5	78.6 (36.0)	H-C5	115.5 (49.6)	H-C5
B) Axial Compression Peaks (−Fy)								
H	44.4 (10.9)	C2-T1	52.2 (2.3)	C4-T1	76.2 (27.0)	C2-T1	74.7 (39.7)	C1-T1
C1	53.3 (6.2)	C3-T1	81.1 (17.4)	C4-T1	112.8 (40.0)	C4-T1	139.9 (32.6)	H,C3-T1
C2	76.0 (14.6)	H,C4-T1	100.6 (14.4)	C6-T1	140.6 (42.8)	H	165.8 (38.6)	H,C5
C3	93.0 (14.8)	H-C1,C6-T1	121.6 (15.1)		158.0 (39.2)	H	202.3 (61.6)	H-C1
C4	107.3 (12.9)	H-C2	136.5 (30.2)	H-C1	169.1 (37.2)	H-C1	218.0 (59.9)	H-C1
C5	103.2 (28.1)	H-C2	133.3 (36.3)	H-C1	169.5 (34.8)	H-C1	223.2 (56.4)	H-C2
C6	112.7 (23.7)	H-C3	140.8 (38.1)	H-C2	166.5 (37.2)	H-C1	214.5 (40.9)	H-C1
C7	114.2 (22.5)	H-C3	143.6 (37.3)	H-C2	166.7 (35.8)	H-C1	205.5 (38.9)	H-C1
T1	114.7 (22.7)	H-C3	144.1 (37.5)	H-C2	167.3 (36.0)	H-C1	206.0 (39.2)	H-C1
C) Posterior Shear Peaks (−Fz)								
H	117.6 (27.6)		145.7 (41.2)		172.7 (43.4)	C7-T1	230.8 (42.3)	
C1	115.8 (26.5)		149.1 (31.5)		167.4 (34.5)	C6-T1	206.6 (29.0)	C7-T1
C2	113.5 (24.0)		144.3 (24.7)		160.3 (39.2)	C6-T1	193.6 (29.9)	C6-T1
C3	114.1 (19.3)		141.1 (22.6)		164.7 (40.7)	C6-T1	185.9 (35.7)	C6-T1
C4	111.6 (17.6)		144.6 (23.5)		175.3 (38.6)	T1	196.7 (42.4)	C6-T1
C5	111.6 (14.9)		146.3 (24.6)		188.2 (38.4)		220.2 (37.5)	
C6	107.4 (13.5)		148.0 (26.3)		203.4 (26.6)	C1-C3	253.0 (22.5)	C2-C4
C7	106.8 (16.0)		148.9 (27.7)		207.2 (26.8)	H-C3	267.7 (22.5)	C2-C4
T1	107.4 (16.3)		150.2 (28.1)		208.5 (27.3)	H-C4	269.5 (23.0)	C1-C4

Table V Rotation peaks (degrees). Average (SD) peak A) flexion and B) extension rotations of H/C1 (head/C1) to C7/T1 during rear impacts of 3.5, 5, 6.5, and 8 g from Panjabi et al. (2005a). Only significantly different values from the pair-wise comparisons between spinal levels are indicated in the column *Significant*. Blank entries indicate that no significant pair-wise comparisons were observed

	3.5 g		5 g		6.5 g		8 g	
	Rotation	Significant	Rotation	Significant	Rotation	Significant	Rotation	Significant
A) Flexion Peaks (+Rx)								
H/C1	4.9 (3.7)	C3/4	5.0 (6.0)		4.4 (5.2)		5.0 (4.7)	
C1/2	2.0 (1.6)		4.4 (4.9)		7.6 (7.3)		9.1 (6.4)	
C2/3	1.5 (1.1)		1.8 (1.0)		3.2 (0.9)		4.0 (1.3)	
C3/4	0.6 (0.4)	H/C1	1.8 (2.2)		3.0 (2.6)		3.1 (2.4)	
B) Extension Peaks (−Rx)								
H/C1	0.8 (1.1)	C4/5,C6/7	9.8 (7.6)		18.3 (10.5)	C1/2	22.3 (11.2)	C1/2-C2/3
C1/2	1.8 (2.1)		4.2 (5.8)		3.8 (3.4)	H/C1	4.2 (2.9)	H/C1
C2/3	4.9 (3.9)		6.2 (4.4)		6.6 (4.3)		6.4 (4.0)	H/C1
C3/4	3.7 (2.0)		5.6 (4.2)		7.6 (6.7)		9.6 (6.3)	
C4/5	9.7 (5.3)	H/C1	11.8 (4.8)		11.7 (4.4)		11.9 (6.2)	
C5/6	8.6 (4.6)		9.2 (6.2)		10.3 (5.8)		10.9 (7.3)	
C6/7	8.9 (6.7)	H/C1	10.5 (7.0)		11.5 (7.7)		12.9 (8.3)	
C7/T1	6.5 (1.2)		8.1 (2.9)		9.5 (2.8)		10.6 (3.4)	

Table VI Translation peaks (mm). Average (SD) peak A) axial separation, B) axial compression, and C) posterior shear translations of H/C1 (head/C1) to C7/T1 during rear impacts of 3.5, 5, 6.5, and 8 g. Only significantly different values from the pair-wise comparisons between spinal levels are indicated in the column *Significant*. Blank entries indicate that no significant pair-wise comparisons were observed

	3.5 g		5 g		6.5 g		8 g	
	Translation	Significant	Translation	Significant	Translation	Significant	Translation	Significant
A) Axial Separation Peaks (+Ty)								
H/C1	16.7 (4.5)	C1/2-C7/T1	26.3 (6.7)	C1/2-C7/T1	28.6 (9.2)	C1/2-C7/T1	30.9 (7.4)	C1/2-C7/T1
C1/2	3.0 (2.1)	H/C1	2.5 (2.4)	H/C1	1.3 (1.8)	H/C1	4.6 (3.2)	H/C1
C2/3	0.4 (0.3)	H/C1	1.7 (1.3)	H/C1	2.6 (2.9)	H/C1	0.9 (0.1)	H/C1
C3/4	2.1 (0.7)	H/C1	1.7 (0.7)	H/C1	1.8 (1.0)	H/C1	1.5 (2.4)	H/C1
C4/5	1.2 (1.0)	H/C1	2.5 (1.3)	H/C1	2.1 (1.9)	H/C1	2.0 (1.9)	H/C1
C5/6	1.6 (1.4)	H/C1	1.8 (1.3)	H/C1	1.8 (1.2)	H/C1	1.8 (1.3)	H/C1
C6/7	1.7 (1.4)	H/C1	0.9 (0.5)	H/C1	1.7 (1.0)	H/C1	1.3 (0.9)	H/C1
C7/T1	0.8 (0.2)	H/C1	0.9 (0.4)	H/C1	2.0 (1.9)	H/C1	2.4 (0.9)	H/C1
B) Axial Compression Peaks (−Ty)								
H/C1	8.3 (3.4)	C1/2-C7/T1	10.0 (2.8)	C1/2-C7/T1	12.5 (4.0)	C2/3-C7/T1	16.7 (5.7)	C1/2-C7/T1
C1/2	3.3 (1.7)	H/C1	3.8 (1.4)	H/C1	3.1 (0.0)		5.4 (1.8)	H/C1
C2/3	2.0 (1.3)	H/C1	2.1 (2.2)	H/C1	1.2 (1.0)	H/C1	1.6 (1.9)	H/C1
C3/4	1.6 (0.8)	H/C1	2.0 (1.8)	H/C1	3.0 (3.6)	H/C1	2.6 (1.7)	H/C1
C4/5	3.7 (2.0)	H/C1	4.6 (2.5)	H/C1	2.4 (0.4)	H/C1	4.8 (3.1)	H/C1
C5/6	1.6 (0.6)	H/C1	1.2 (0.8)	H/C1	3.1 (2.5)	H/C1	2.1 (1.6)	H/C1
C6/7	0.9 (0.3)	H/C1	1.1 (0.5)	H/C1	3.7 (3.5)	H/C1	3.6 (3.2)	H/C1
C7/T1	3.8 (3.4)	H/C1	2.6 (1.7)	H/C1	4.6 (2.6)	H/C1	3.2 (1.8)	H/C1
C) Posterior Shear Peaks (−Tz)								
H/C1	39.3 (5.9)	C1/2-C7/T1	59.9 (19.1)	C1/2-C7/T1	74.2 (22.7)	C1/2-C7/T1	83.3 (17.0)	C1/2-C7/T1
C1/2	11.7 (4.4)	H/C1,C5/6-C6/7	12.9 (5.6)	H/C1	14.6 (7.2)	H/C1	13.3 (5.6)	H/C1
C2/3	10.3 (1.9)	H/C1,C6/7-C7/T1	11.6 (2.4)	H/C1	13.9 (3.0)	H/C1	12.8 (3.3)	H/C1
C3/4	9.5 (3.5)	H/C1,C6/7-C7/T1	11.7 (4.2)	H/C1	13.6 (4.2)	H/C1	11.3 (4.1)	H/C1
C4/5	9.1 (1.9)	H/C1,C6/7-C7/T1	9.7 (2.4)	H/C1	10.8 (2.1)	H/C1,C7/T1	10.7 (2.5)	H/C1
C5/6	5.9 (3.2)	H/C1-C1/2,C7/T1	8.1 (4.5)	H/C1-C7/T1	8.7 (4.6)	H/C1,C7/T1	7.6 (4.6)	H/C1,C7/T1
C6/7	3.5 (1.7)	H/C1-C4/5,C7/T1	4.6 (2.1)	H/C1-C7/T1	4.9 (2.0)	H/C1,C7/T1	6.3 (2.9)	H/C1,C7/T1
C7/T1	16.3 (3.4)	H/C1,C2–3-C67	23.3 (8.7)	H/C1,C5/6-C6/7	28.7 (11.8)	H/C1,C4/5-C6/7	25.5 (7.8)	H/C1,C5/6-C6/7

Table VII Event Times (ms). Average (SD) times at which the peak loads and motions were attained at A) H/C1 (head/C1) to C3/4 and B) C4/5 to C7/T1, relative to the onset of the T1 horizontal acceleration during the 5 g rear impact. The average magnitudes of the peak loads (Nm or N) and motions (degrees or mm) are also provided. For each spinal level, the times of the peak loads at the CoM of the upper mass and the peak intervertebral motions are reported in chronological order. The loads are indicated with italicized bold

Time	Event H/C1	Magnitude	Time	Event C1/2	Magnitude	Time	Event C2/3	Magnitude	Time	Event C3/4	Magnitude
A) H/C1 to C3/4											
60.3 (5.6)	***+Mx***	***3.7***	70.0 (17.0)	***+Mx***	***1.7***	58.0 (0.0)	***+Mx***	***1.6***	58.0 (0.0)	***+Mx***	***1.0***
86.0 (10.3)	***+Fy***	***139.7***	83.3 (7.8)	***+Fy***	***109.8***	76.4 (7.9)	+Rx	1.8	82.3 (8.1)	***+Fy***	***87.6***
115.7 (22.4)	+Rx	5.0	114.7 (72.2)	+Rx	4.4	83.3 (8.5)	***+Fy***	***101.5***	108.7 (14.7)	***−Fz***	***141.1***
126.0 (15.0)	***−Fz***	***145.7***	116.3 (9.9)	***−Fz***	***149.1***	113.7 (12.9)	***−Fz***	***144.3***	113.2 (79.1)	+Rx	1.8
129.0 (16.7)	+Ty	26.3	132.0 (23.5)	−Tz	12.9	136.3 (25.1)	***−Mx***	***21.0***	126.0 (14.2)	***−Mx***	***23.3***
149.7 (37.5)	***−Mx***	***5.6***	152.0 (59.0)	***−Fy***	***81.1***	139.2 (45.3)	***−Fy***	***100.6***	138.8 (45.5)	***−Fy***	***121.6***
173.7 (45.1)	−Tz	59.9	152.3 (45.5)	***−Mx***	***18.7***	150.0 (38.9)	−Tz	11.6	141.3 (16.2)	+Ty	1.7
198.0 (31.1)	***−Fy***	***52.2***	164.5 (73.3)	+Ty	2.5	156.0 (34.2)	−Rx	6.2	155.6 (53.7)	−Tz	11.7
198.7 (50.1)	−Rx	9.8	181.3 (33.0)	−Rx	4.2	171.5 (74.3)	−Ty	2.1	158.7 (83.1)	−Rx	5.6
241.5 (36.2)	−Ty	10.0	250.7 (60.9)	−Ty	3.8	199.0 (91.9)	+Ty	1.7	256.5 (61.5)	−Ty	2.0
	C4/5			C5/6			C6/7			C7/T1	
B) C4/5 to C7/T1											
80.7 (8.0)	***+Fy***	***77.3***	78.7 (7.0)	***+Fy***	***65.6***	89.7 (10.5)	***−Fz***	***148.0***	87.7 (8.8)	***−Fz***	***148.9***
103.0 (16.6)	***−Fz***	***144.6***	100.3 (17.0)	***−Fz***	***146.3***	105.7 (74.8)	***+Fy***	***43.4***	89.3 (7.0)	+Ty	0.9
126.0 (13.2)	***−Mx***	***25.6***	125.3 (13.1)	***−Mx***	***27.9***	124.7 (13.4)	***−Mx***	***29.5***	111.7 (25.8)	−Rx	8.1
138.4 (45.7)	***−Fy***	***136.5***	141.0 (41.7)	***−Fy***	***133.3***	125.0 (15.4)	***−Fy***	***140.8***	122.3 (76.9)	***+Fy***	***36.7***
145.7 (40.7)	−Tz	9.7	161.0 (44.9)	−Rx	9.2	145.7 (43.3)	−Tz	4.6	123.7 (15.1)	***−Fy***	***143.6***
164.0 (38.1)	−Rx	11.8	172.3 (62.3)	−Tz	8.1	150.0 (35.7)	−Rx	10.5	124 (13.4)	***−Mx***	***30.8***
214.5 (77.6)	−Ty	4.6	177.0 (34.5)	−Ty	1.2	183.7 (75.8)	−Ty	1.1	197.3 (57.7)	−Ty	2.6
215.0 (86.3)	+Ty	2.5	190.5 (66.8)	+Ty	1.8	199.0 (97.4)	+Ty	0.9	276.3 (46.9)	−Tz	23.3

intervertebral translations were calculated at the CoMs of the head and vertebrae. The peak motions generally increased with increasing impact acceleration. +Rx peaks were not observed inferior to C3/4 (Table VA). The highest +Rx peak of 9.1° was observed at C1/2, while highest the −Rx peak of 22.3° (Table VB) was observed at head/C1, both during the 8 g impact. The +Ty and −Ty peaks at head/C1, reaching 30.9 and 16.7 mm, respectively, were significantly greater than at all other intervertebral levels, during all impacts except 6.5 g (Tables VIA and VIB). The −Tz peaks were generally greatest at head/C1, followed by C7/T1 (Table VIC). The Tz peaks at head/C1 were significantly greater than at all other intervertebral levels, during all impacts.

Temporal Analyses. The average times at which peak loads and motions were attained during the 5 g rear impact are presented in tabular form, ordered chronologically for each spinal level (Tables VIIA and VIIB). At head/C1 to C3/4 (Table VIIA), the peak loads of +Mx and +Fy occurred first, prior to the peak motion of +Rx, except at C2/3, where peak +Fy occurred following peak +Rx. Subsequently, at C2/3, the peak loads of −Fz, −Mx, and −Fy occurred, followed by the peak motions of −Tz, −Rx, and ±Ty. At C4/5 to C7/T1 (Table VIIB), the peak loads of +Fy, −Fz, −Mx, and −Fy occurred prior to the peak motions of −Tz, −Rx, and ±Ty, except at C7/T1, where the ±Fy and −Mx peaks occurred following the +Ty and −Rx peaks.

DISCUSSION

Disability and chronic pain due to soft-tissue neck injury caused by automotive collisions remains an important societal problem (Jakobsson et al., 2000; Spitzer et al., 1995). To better understand neck-injury mechanisms, it is necessary to know both the dynamic motions and loads at each spinal level as the impact energy moves caudally from the head. Although the motions have been studied in numerous investigations (Cusick et al., 2001; Panjabi et al., 2005a), practically nothing is known about the magnitudes, caudal progression, and timing of the dynamic vertebral loads. The previous studies are limited to determination of the dynamic loads at the occipital condyles or T1 vertebra during simulated rear impacts (Mertz & Patrick, 1967; Siegmund et al., 2001; Tencer et al., 2002; Yoganandan et al., 2000). Ours is the first study to provide comprehensive simultaneous dynamic vertebral load and motion data, using a previously described and validated experimental model (Ivancic et al., 2005b). In a representative example of rear impact (Figures 4A to 4C), the initial loads included flexion moments at head and C3 and an extension moment at C6, combined with forces of axial tension and posterior shear. At head/C1, these loads caused flexion rotation and translations of axial separation and posterior shear. Subsequently, C3 and C6 experienced combined extension moments and forces of axial compression and posterior shear. These loads caused extension rotation and posterior shear translation at C3/4 and extension rotation at C6/7.

The temporal analyses of the average peak loads and motions for each spinal level during the 5 g rear impact are provided in Table VII. Immediately following impact, the loads included a combined flexion moment and axial tension force at head to C3, which caused flexion rotation of head/C1 to C3/4. Subsequently, at C4/5 to C6/7, the combined loads of extension moment and forces of posterior shear and axial compression caused motions

of extension rotation and posterior and axial compression translations. These load-motion patterns are in agreement with results of a previous biomechanical study that reported intervertebral motions of the C2/3 to C7/T1 spinal levels in response to quasi-static forces (Panjabi et al., 1986). They found that axial tension force caused flexion rotation, while axial compression and posterior shear forces, each independently applied, caused extension rotation, and axial compression and posterior shear translations. The present results may provide important new insight into the load-motion patterns causing neck injury during whiplash. Immediately following impact, head/C1 to C3/4 were loaded with a combined flexion moment and axial tension force causing flexion rotation. At C4/5 to C6/7, combined extension moment and posterior shear and axial tension forces caused extension rotation and posterior shear translation. The posterior shear force peaks were larger than the axial tension peaks. Subsequently, the entire cervical spine was loaded in combined extension moment and forces of posterior shear and axial compression, which caused extension rotation and posterior and axial translation.

Significant differences ($P < 0.05$) in the average peak dynamic loads (Tables IIIA to IVC) and motions (Tables VA to VIC) throughout the cervical spine were observed. Among the dynamic loads, the extension moment peaks at C4 to T1 exceeded the peaks at the head and C1. The axial tension peaks at head to C4 were greater than at C6 to T1, while the axial compression peaks at C4 to T1 exceeded the peaks at head to C1. The posterior shear force peaks were greater at C6 to T1, as compared to C2 to C4, during the 8 g impact. Among the dynamic motions, the translations were greatest at head/C1, as compared to other spinal levels.

The limitations of the present study must be considered before the results may be applied to reduce neck injuries in real-life rear impacts. Every attempt was made to mount the cervical spine specimens in a consistent neutral posture, however some differences existed among specimens due to anatomical constraints and mounting difficulties (Table IA). The T1 vertebra was fixed to the trauma sled, which may have affected the cervical spine loads and motions, particularly at C7/T1. The incremental trauma approach was utilized in order to determine the relation between the dynamic cervical spine loads and motions and the impact acceleration. The incremental and single trauma protocols (both achieving the same final trauma) have been shown to produce equivalent soft-tissue injury severity due to whiplash-type impacts in a porcine cervical spine model (Ghole et al., 2004). The effects of the neuromuscular control system on the calculated cervical spine loads were not modeled. The present MFR provided passive stability and resistance to dynamic intervertebral motions, producing a kinematic response to rear-impact loading similar to in vivo data (Ivancic et al., 2005b). To calculate the cervical spine loads, the present inverse dynamics model utilized generic vertebral masses and sagittal mass moments of inertia (Camacho et al., 1997) and a surrogate head with standard mass and mass moment of inertia (Table IB). The remaining input data were specific to each specimen, including the dynamic head and vertebral kinematics, accelerations, and load-cell data. The statistical analyses investigated differences in the average peak loads and motions between spinal levels for each impact. Statistical relations and differences in load and motion coupling patterns were not investigated.

How do the present results compare with previously reported in vivo data? The present average peak loads at the CoMs of the head and C1 during the 3.6 g impact of the T1 vertebra may be compared and contrasted with the previously reported in vivo dynamic loads at the occipital condyles. These comparisons should be made cautiously, since the in vivo studies expressed the forces at the occipital condyles in the head coordinate system, while the present study expressed the forces at the CoM of the head in the C1 anatomic coordinate system. Siegmund et al. (2001) performed simulated rear impacts using volunteers seated in automobiles with head restraints. Vehicle speed changes up to 8.0 kph resulted in measured peak T1 horizontal accelerations between 2.5 and 3.8 g. They reported average (SD) peak loads at the occipital condyles of 14.5 (4.0) Nm for extension moment, 138.8 (47.8) N for posterior shear, and 503.2 (59.7) N for axial tension. The former two loads are in excellent agreement with the presently reported 13.6 Nm moment at C1 (Table IIIB), and 117.6 N posterior shear at the head (Table IVC). However, the present 84.1 N axial tension at the head (Table IVA) is much less than the in vivo peak. This difference may be due to differences in experimental designs, as Siegmund et al. (2001) used a head restraint, while the present study did not. The present data are also in good agreement with those reported in previous studies that impacted volunteers seated in rigid automobile seats on an inclined sled without a head restraint, with measured peak T1 horizontal accelerations between 3.0 and 4.0 g (Davidsson et al., 1999; Ono et al., 1997). Ono et al. (1997) reported peaks of 8 Nm for moment, 100 N for posterior shear, and 125 N for axial tension, while Davidsson et al. (1999) reported peaks of 2 to 6 Nm for moment, 50 to 125 N for posterior shear, and 100 to 300 N for axial tension.

Is it possible for the neck muscles to achieve sufficient force to resist the dynamic vertebral loads during whiplash? The present highest average peak dynamic extension moments at C1, C4, and T1, of 29.2, 37.4, and 40.7 Nm, respectively, during the 8 g impact, may be compared against the in vivo physiological capacity to resist such moments. In a study of the isometric strength of the human neck muscles, Vasavada et al. (2001) found that men were stronger than women and could generate average peak flexion moments of 13, 19, and 30 Nm, at head/C1, C4, and C7/T1, respectively, while the corresponding peaks for women reached 6, 10, and 15 Nm (Vasavada et al., 2001). Based upon the C7/T1 data alone, the anterior cervical muscles may not be able to develop sufficient strength to counteract the dynamic extension moment to protect the neck ligaments from injury during whiplash. Women may fail during impacts of less than 3.5 g, while men may barely be able to resist 5 g impacts. These observations are also supported by a recent in vitro biomechanical study that reported the 5 g impact as the threshold for the onset

of subfailure injury to the anterior cervical spine ligaments in a mixed group of male and female specimens (Ito et al., 2004).

At what magnitude of dynamic extension moment does neck injury occur? The present highest average peak dynamic extension moments may be compared against the proposed tolerance limits (Mertz & Patrick, 1967, 1971; Nightingale et al., 2002). Based upon observations of gross neck-ligament injuries in cadavers due to simulated rear impacts in earlier studies, Mertz and Patrick (1967, 1971) observed gross injuries with a dynamic extension moment of 57 Nm at the occipital condyles, while below 47 Nm there were no injuries. The shear and axial forces did not correlate with injury. The extension moment was not calculated throughout the cervical spine, thus precluding determination of the failure moment tolerances specific to each spinal level. These data are contrasted by Nightingale et al. (2002) who found extension failure moments of 43.3 Nm for occiput-C2 specimens and 21.2 Nm for C3/4 to C7/T1 spinal levels. The present peak C1 extension moment of 29.2 Nm during the 8 g impact was below the failure limit of 43.3 Nm, indicating no potential for injury. Alternatively, the failure limit of 21.2 Nm for C3/4 to C7/T1 was exceeded in the present study beginning at 3.5 g (Table IIIB), indicating the potential for ligamentous injury at the middle and lower cervical spine even at low-impact accelerations.

The present results may provide important motivation for the development of new anthropometric test dummies. Current evaluation of automotive injury-prevention systems for predicting injury due to rear impact is commonly performed through crash testing of existing anthropometric test dummies, such as the Hybrid III or BioRID II (Schmitt et al., 2002; Zuby et al., 1999). The dynamic load and motion biofidelity and injury prediction of either neck surrogate have not been validated. The present vertebral load and motion data may be useful for developing potential injury corridors. The new biofidelic anthropometric test dummies capable of dynamic vertebral load and intervertebral motion measurements, together with the validated injury potential corridors, will be superior to the present-day dummies.

Another use of the present data may be towards the development of an improved vertebral load-based neck-injury criteria (VL-NIC). The normalized Neck Injury Criterion (Nij) (Eppinger et al., 1999, 2000) and the Neck Protection Criterion (Nkm) (Schmitt et al., 2002), consider only the upper neck dynamic loads. These criteria have been developed, most likely due to the ease by which a load cell may be positioned in the upper neck surrogate of the present test dummies. The VL-NIC would complement the existing motion based criterion, for example the Intervertebral Neck Injury Criterion (IV-NIC) (Panjabi et al., 2005a) and the Neck Displacement Criterion (NDC) (Viano & Davidsson, 2002). The IV-NIC has been correlated with soft-tissue neck injury severity, and can predict the intervertebral level, severity, time, and mode of injury during simulated impacts (Ivancic et al., 2005a; Ivancic et al., 2006a; Panjabi et al., 2005a; Panjabi et al., 2005b). The combined vertebral load and motion based injury criteria may be helpful towards the development of more efficient neck-injury prevention systems.

CONCLUSIONS

The dynamic loads and intervertebral motions were calculated throughout the cervical spine during simulated rear impacts of 3.5, 5, 6.5, and 8 g using the whole human cervical spine model with muscle force replication and surrogate head. The interplay between loads, motions and timing was complex. During the 5 g impacts, the first loads to occur at head to C3 were a combination of flexion moment and axial tension force causing flexion rotation. Subsequently, these spinal levels experienced extension moment and forces of axial compression and posterior shear. These loads caused intervertebral extension rotation and translation of posterior shear and axial separation, followed by axial compression. At C4 to C6, combined peak loads of extension moment and forces of posterior shear and axial compression occurred prior to all the intervertebral motion peaks. Based upon data from all the impacts, the extension moment and axial compression force peaks at C4 to T1 were significantly greater than at the upper cervical spine. The axial tension force peaks at head to C4 significantly exceeded the peaks at C6 to T1. The posterior shear force peaks were generally greater at the lower cervical spine, as compared to the middle. The present data improves our understanding of the head and neck loads and motions during whiplash and may lead to future development of new anthropometric test dummies, vertebral load-based neck-injury criteria, and more effective neck-injury prevention systems.

ACKNOWLEDGMENTS

This research was supported by the NIH Grant 1 RO1 AR45452 1A2.

REFERENCES

Becker E. (1972) Measurement of Mass Distribution Parameters of Anatomic Segments, Paper No. 720964: Society of Automotive Engineers, Warrendale, PA.

Camacho DL, Nightingale RW, Robinette JJ, Vanguri SK, Coates DJ, Myers BS. (1997) Experimental Flexibility Measurements for the Development of a Computational Head-Neck Model Validated for Near-Vertex Head Impact, Paper No. 973345: Society of Automotive Engineers, Warrendale, PA.

Cusick JF, Pintar FA, Yoganandan N. (2001) Whiplash Syndrome: Kinematic Factors Influencing Pain Patterns. *Spine*, Vol. 26, pp. 1252–1258.

Davidsson J, Lovsund P, Ono K, Svensson M, Inami S. (1999) A Comparison Between Volunteer, BioRID P3 and Hybrid III Performance in Rear Impacts. *International Research Council on Biomechanics of Impact*, Sitges, Spain, pp. 165–178.

Eppinger R, Sun E, Kuppa S, Saul R. (1999, 2000) *Supplement: Development of Improved Injury Criteria for Assessment of Advanced Automotive Restraint Systems—II*, Washington, DC: US DOT/National Highway Traffic Safety Administration.

Freeman MD, Croft AC, Rossignol AM, Weaver DS, Reiser M. (1999) A Review and Methodologic Critique of the Literature Refuting Whiplash Syndrome. *Spine*, Vol. 24, pp. 86–96.

Garcia T, Ravani B. (2003) A Biomechanical Evaluation of Whiplash Using a Multi-Body Dynamic Model. *J. Biomech. Eng.*, Vol. 125, pp. 254–265.

Ghole SA, Ivancic PC, Tominaga Y, Gimenez SE, Panjabi MM. (2004) Incremental and Single Trauma Produce Equivalent Subfailure Soft Tissue Injury of the Cervical Spine. *Clin. Biomech.*, Vol. 19, pp. 784–789.

Ito S, Ivancic PC, Panjabi MM, Cunningham BW. (2004) Soft Tissue Injury Threshold During Simulated Whiplash: A Biomechanical Investigation. *Spine*, Vol. 29, pp. 979–987.

Ivancic PC, Ito S, Panjabi MM, Pearson AM, Tominaga Y, Wang JL, Gimenez SE. (2005a) Intervertebral Neck Injury Criterion for Simulated Frontal Impacts. *Traffic Inj. Prev.*, Vol. 6, pp. 175–184.

Ivancic PC, Panjabi MM, Ito S, Cripton PA, Wang JL. (2005b) Biofidelic Whole Cervical Spine Model With Muscle Force Replication for Whiplash Simulation. *Eur. Spine J.*, Vol. 14, pp. 346–355.

Ivancic PC, Panjabi MM, Tominaga Y, Malcolmson GF. (2006a) Predicting Multiplanar Cervical Spine Injury Due to Head-Turned Rear Impacts Using IV-NIC. *Traffic Inj. Prev.*, Vol. 7, pp. 264–275.

Ivancic PC, Wang JL, Panjabi MM. (2006b) Calculation of Dynamic Spinal Ligament Deformation. *Traffic Inj. Prev.*, Vol. 7, pp. 81–87.

Jakobsson L, Lundell B, Norin H, Isaksson-Hellman I. (2000) WHIPS—Volvo's Whiplash Protection Study. *Accid. Anal. Prev.*, Vol. 32, pp. 307–319.

Luan F, Yang KH, Deng B, Begeman PC, Tashman S, King AI. (2000) Qualitative Analysis of Neck Kinematics During Low-Speed Rear-End Impact. *Clin. Biomech.*, Vol. 15, pp. 649–657.

Mertz HJ, Patrick LM. (1967) *Investigation of the Kinematics and Kinetics of Whiplash*, Paper No. 670919: Society of Automotive Engineers, Warrendale, PA.

Mertz HJ, Patrick LM. (1971) Strength and Response of the Human Neck, Paper 710855, Warrendale, PA: Society of Automotive Engineers.

Nightingale RW, Winkelstein BA, Knaub KE, Richardson WJ, Luck JF, Myers BS. (2002) Comparative Strengths and Structural Properties of the Upper and Lower Cervical Spine in Flexion and Extension. *J. Biomech.*, Vol. 35, pp. 725–732.

Ono K, Kaneoka K, Wittek A, Kajzer J. (1997) Cervical Injury Mechanism Based on the Analysis of Human Cervical Vertebral Motion and Head-Neck-Torso Kinematics During Low Speed Rear Impacts, Paper No. 973340. Warrendale, PA: Society of Automotive Engineers.

Panjabi MM, Summers DJ, Pelker RR, Videman T, Friedlaender GE, Southwick WO. (1986) Three-Dimensional Load-Displacement Curves Due to Forces on the Cervical Spine. *J. Orthop. Res.*, Vol. 4, pp. 152–161.

Panjabi MM, Cholewicki J, Nibu K, Babat LB, Dvorak J. (1998) Simulation of Whiplash Trauma Using Whole Cervical Spine Specimens. *Spine*, Vol. 23, pp. 17–24.

Panjabi MM, Ito S, Pearson AM, Ivancic PC. (2004a) Injury Mechanisms of the Cervical Intervertebral Disc During Simulated Whiplash. *Spine*, Vol. 29, pp. 1217–1225.

Panjabi MM, Pearson AM, Ito S, Ivancic PC, Wang JL. (2004b) Cervical Spine Curvature During Simulated Whiplash. *Clin. Biomech.*, Vol. 19, pp. 1–9.

Panjabi MM, Ito S, Ivancic PC, Rubin W. (2005a) Evaluation of the Intervertebral Neck Injury Criterion Using Simulated Rear Impacts. *J. Biomech.*, Vol. 38, pp. 1694–1701.

Panjabi MM, Ivancic PC, Tominaga Y, Wang JL. (2005b) Intervertebral Neck Injury Criterion for Prediction of Multiplanar Cervical Spine Injury Due to Side Impacts. *Traffic Inj. Prev.*, Vol. 6, pp. 387–397.

Pearson AM, Ivancic PC, Ito S, Panjabi MM. (2004) Facet Joint Kinematics and Injury Mechanisms During Simulated Whiplash. *Spine*, Vol. 29, pp. 390–397.

Schmitt K-U, Muser MH, Walz FH, Niederer PF. (2002) Nkm—A Proposal for a Neck Protection Criterion for Low-Speed Rear-End Impacts. *Traffic Inj. Prev.*, Vol. 3, pp. 117–126.

Siegmund GP, Heinrichs BE, Lawrence JM, Philippens M. (2001) Kinetic and Kinematic Responses of the RID2a, Hybrid III and Human Volunteers in Low-Speed Rear-End Collisions, Paper No. 2001-22-0011, Warrendale, PA: Society of Automotive Engineers.

Spitzer WO, Skovron ML, Salmi LR, Cassidy JD, Duranceau J, Suissa S, Zeiss E. (1995) Scientific Monograph of the Quebec Task Force on Whiplash-Associated Disorders: Redefining "Whiplash" and Its Management. *Spine*, Vol. 20, pp. 1S–73S.

Stemper BD, Yoganandan N, Pintar FA. (2003) Kinetics of the Head-Neck Complex in Low-Speed Rear Impact. *Biomed. Sci. Instrum.*, Vol. 39, pp. 245–250.

Tencer AF, Mirza S, Bensel K. (2002) Internal Loads in the Cervical Spine During Motor Vehicle Rear-End Impacts: the Effect of Acceleration and Head-to-Head Restraint Proximity. *Spine*, Vol. 27, pp. 34–42.

van den Kroonenberg A, Philippens M, Cappon H, Wismans J, Hell W, Langwieder K. (1998) Human Head-Neck Response During Low-Speed Rear End Impacts, Paper No. 983158, Warrendale, PA: Society of Automotive Engineers.

van der Horst M. (2002) Human Head Neck Response in Frontal, Lateral and Rear End Impact Loading: Modelling and Validation. Ph.D. Dissertation. Eindhoven, The Netherlands: Eindhoven University of Technology.

Vasavada AN, Li S, Delp SL. (2001) Three-Dimensional Isometric Strength of Neck Muscles in Humans. *Spine*, Vol. 26, pp. 1904–1909.

Viano DC, Davidsson J. (2002) Neck Displacements of Volunteers, BioRID P3 and Hybrid III in Rear Impacts: Implications to Whiplash Assessment by a Neck Displacement Criterion (NDC). *Traffic Inj. Prev.*, Vol. 3, pp. 105–116.

Walker L, Harris E, Pontius U. (1973) Mass, Volume, Center of Mass, and Mass Moment of Inertia of Head and Neck of Human Body, Paper No. 730985, Society of Automotive Engineers.

White AA, 3rd, Panjabi MM. (1990) *Clinical Biomechanics of the Spine*, Philadelphia: J.B. Lippincott Co.

Yoganandan N, Pintar F, Stemper BD, Schlick MB, Philippens M, Wismans J. (2000) Biomechanics of Human Occupants in Simulated Rear Crashes: Documentation of Neck Injuries and Comparison of Injury Criteria, Paper No. 2000-01-SC14: Society of Automotive Engineers.

Yoganandan N, Pintar FA. (1997) Inertial Loading of the Human Cervical Spine. *J. Biomech. Eng.*, Vol. 119, pp. 237–240.

Zuby DS, Troy Vann D, Lund AK, Morris CR. (1999) Crash Test Evaluation of Whiplash Injury Risk, Paper No. 99SC17: Society of Automotive Engineers.